https://doi.org/ 10.70882/ytdzj843

SCIENCE FORUM (JOURNAL OF PURE AND APPLIED SCIENCES) 26, (4) (2026), 436 - 450

Science Forum (Journal of Pure and Applied Sciences)

Journal Homepage: https://atbuscienceforum.com.ng/index.php/jpas

Numerical Investigation of Tip Speed Ratio Effects on the Performance of a Jet-Driven Four-Bladed Waterwheel for Low-Head Hydropower Applications

Raji, Adebayo Idowu[1], Ladokun, Laniyi Laniran[2]*, Adeboye, Buliaminu Ademola[1], Abdulraheem, Jimoh Tunde[1], Olatinwo, Toyyibah Folake[1]

[1] Department of Mechatronics Engineering, Kwara State Polytechnic, Ilorin, Kwara State, Nigeria

[2] Turbo-machines Design and Construction Unit, National Centre for Hydropower Research and Development, Energy Commission of Nigeria, University of Ilorin, Ilorin, Kwara State, Nigeria

Abstract

This study presents a numerical investigation of the influence of Tip Speed Ratio (TSR) on the hydrodynamic and energy-conversion performance of a jet-driven, four-bladed waterwheel designed for low-head hydropower applications using transient Computational Fluid Dynamics (CFD). A two-dimensional transient numerical model was developed in ANSYS Fluent, employing the Shear Stress Transport (SST) *k–ω* turbulence model to capture the unsteady interaction between the incoming water jet and the rotating runner blades. Simulations were performed under eight operating conditions, corresponding to runner rotational speeds ranging from 10 to 45 rpm, while maintaining a constant inlet jet velocity of 3.0 m/s. Transient torque histories obtained from the simulations were analysed to determine average torque, mechanical power, hydraulic efficiency, power coefficient, and the corresponding TSR for each operating condition. The results demonstrate a strong dependence of waterwheel performance on TSR. The highest average torque of 169.48 Nm was recorded at 10 rpm (TSR = 0.244). In contrast, optimum energy-conversion performance occurred at 35 rpm, where the maximum mechanical power of 489.72 W, hydraulic efficiency of 60.57%, and power coefficient of 0.606 were achieved at an optimum TSR of 0.855. The transient torque profiles exhibited characteristic periodic oscillations associated with successive blade–jet interactions during runner rotation. These findings demonstrate that operating the waterwheel near its optimum TSR substantially enhances energy extraction and conversion efficiency. The results provide useful technical guidance for the design, operational optimization, and performance improvement of jet-driven waterwheels intended for decentralized and sustainable low-head hydropower generation.

Keywords
Tip Speed Ratio (TSR);
Jet-driven waterwheel;
Low-head hydropower;
Computational Fluid Dynamics (CFD);
Hydraulic performance.

EISSN: 3156-5190 (Online)
ISSN: 1119-4618 (Print)
JPAS
Faculty of Science, ATBU Bauchi

Corresponding Author: Ladokun, Laniyi Laniran, Turbo-machines Design and Construction Unit, National Centre for Hydropower Research and Development, Energy Commission of Nigeria, University of Ilorin, Ilorin, Kwara State, Nigeria. Email: ladokunll.nachred@unilorin.edu.ng

1. INTRODUCTION

Recent global efforts toward sustainable energy development have generated renewed interest in low-head hydropower technologies capable of harnessing the vast but underutilized energy potential of rivers, irrigation canals, and water transmission systems. Among such technologies, waterwheels have emerged as attractive alternatives to conventional hydraulic turbines due to their simplicity, low environmental impact, ease of fabrication, and suitability for decentralized power generation (Quaranta & Revelli, 2018; Štigler, 2022). Recent research has gradually focused on understanding the hydrodynamic behavior and performance optimization of waterwheels through both experimental and numerical investigations (Asim et al., 2022; Shingala et al., 2022; Cleynen et al., 2021).

One of the most important parameters influencing the performance of waterwheels is the ratio between wheel tangential velocity and incoming water velocity, commonly expressed as the Tip Speed Ratio (TSR). The TSR governs the interface between the moving blades and the incident flow, creating effects on the torque generation, energy transfer, and overall hydraulic efficiency. In an experimental investigation of undershot waterwheels, Buku and Yandi (2026) demonstrated that wheel performance is highly dependent on the ratio of wheel tangential velocity to upstream flow velocity. Their findings showed an optimal operating range in which momentum transfer from the flow to the wheel is maximized, while excessively low or high rotational speeds lead to reduced hydraulic efficiency. These observations highlight the importance of TSR optimization in waterwheel design and operation.

Advances in computational fluid dynamics have enabled increasingly detailed investigations of hydraulic energy converters. Numerical simulations provide valuable insights into velocity distributions, pressure fields, vortex structures, turbulence characteristics, and transient blade-flow interactions. For example, Paudel et al. (2022) employed CFD techniques to investigate hydraulic performance and internal flow characteristics of waterwheel systems, demonstrating that numerical models can accurately predict performance trends while providing information that is difficult to obtain experimentally.

Transient CFD simulations have been widely used to evaluate hydropower devices, demonstrating their effectiveness for performance prediction and design optimization. However, most studies have focused on conventional waterwheels rather than jet-driven designs. Jet-driven waterwheels remain poorly investigated. Unlike conventional waterwheels that extract energy from flowing water, they rely on the momentum of a directed water jet striking the blades, producing localized impact forces and greater sensitivity to tip speed ratio (TSR) (Basar et al., 2025). Although impulse turbines such as Pelton and Banki have been extensively studied, limited research has examined jet-driven waterwheels under varying TSRs, particularly four-bladed configurations.

The available literature therefore reveals several important research gaps. First, although numerous studies have investigated conventional waterwheel systems, limited attention has been devoted to jet-driven waterwheels operating under low-head conditions (Jiang et al., 2025). Second, there remains insufficient understanding of the influence of TSR on the transient torque behavior, power output, and energy conversion characteristics of low-solidity four-bladed waterwheels.

Third, detailed CFD-based analyses examining blade-flow interactions and performance optimization in jet-driven waterwheel systems remain relatively scarce. Addressing these gaps is essential for improving the design and operational efficiency of low-cost hydropower devices intended for rural electrification and decentralized energy generation.

Consequently, the present study numerically investigates the effect of Tip Speed Ratio on the performance of a jet-driven four-bladed waterwheel designed for low-head hydropower applications. The findings are expected to contribute to the growing body of knowledge on sustainable low-head hydropower technologies while providing practical design guidelines for the development of efficient jet-driven waterwheel systems.

2. Materials and Methods

2.1 Numerical Model Description

The hydrodynamic performance of a jet-driven four-bladed waterwheel was investigated using Computational Fluid Dynamics (CFD). A two-dimensional transient numerical model was developed to simulate the interaction between a free water jet and the rotating runner under various operating conditions corresponding to different Tip Speed Ratios (TSRs). The numerical approach allows for in-depth analysis of the transient flow behaviour, pressure distribution, velocity field, and torque characteristics associated with the waterwheel operation.

The numerical domain consisted of a stationary fluid region containing a rotating circular sub-domain within which the waterwheel was located. The rotating sub-domain employed a sliding mesh technique to accurately capture the transient interaction between the moving blades and the incoming water jet. The waterwheel runner comprised four identical curved blades symmetrically distributed around a central hub. The blade profile was selected to allow the incoming jet to impinge on the inner concave surface of each blade, thereby maximizing momentum transfer and producing clockwise rotation. The computational domain was designed sufficiently large to minimize the influence of boundary conditions on the flow field. The turbine centre was located at the origin of the coordinate system, while adequate upstream and downstream distances were maintained to allow complete jet development before blade impact and wake dissipation after energy extraction.

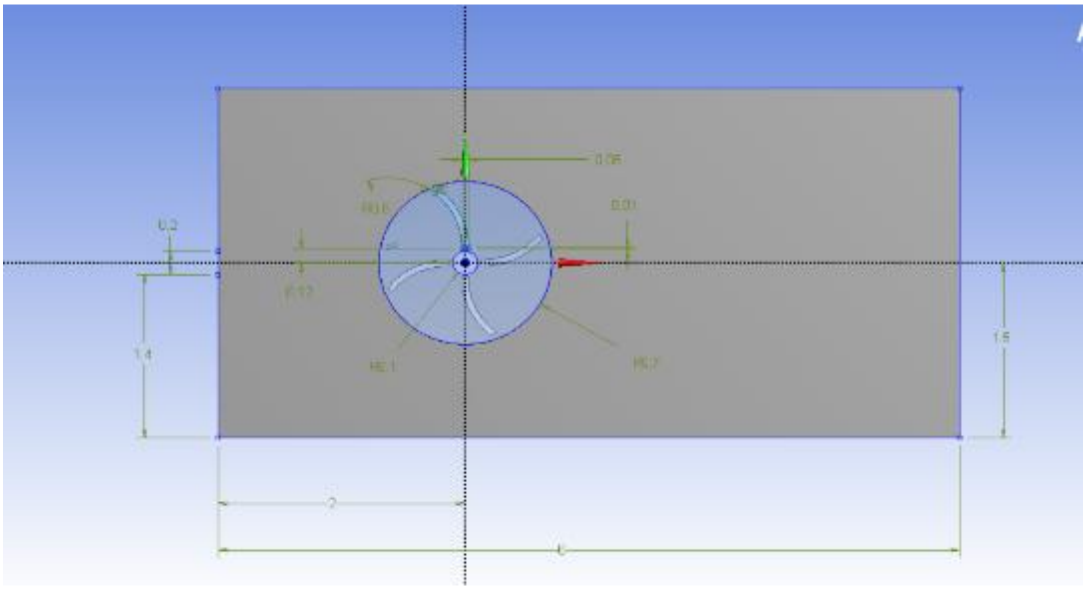

Figure 1. Computational geometry of the jet-driven waterwheel

2.2 Computational Geometry

The principal geometric parameters employed in the numerical model are summarized in Table 1.

Table 1: Geometrical parameters of the numerical model.

Parameter	Value
Runner diameter	1.40 m
Runner radius	0.70 m
Runner width (prototype depth)	0.30 m
Number of blades	4
Computational model	Two-dimensional
Computational domain length	4.75 m
Distance from runner centre to inlet boundary	0.75 m
Distance from runner centre to outlet boundary	4.00 m
Inlet opening height	0.20 m
Inlet elevation above lower boundary	1.70 m
Rotational direction	Clockwise

The inlet was positioned on the left boundary of the computational domain with a vertical opening of 0.20 m located 1.70 m above the lower wall. This configuration allowed the water jet to strike the inner curved surface of the blades, thereby reproducing the operating principle of a jet-driven waterwheel.

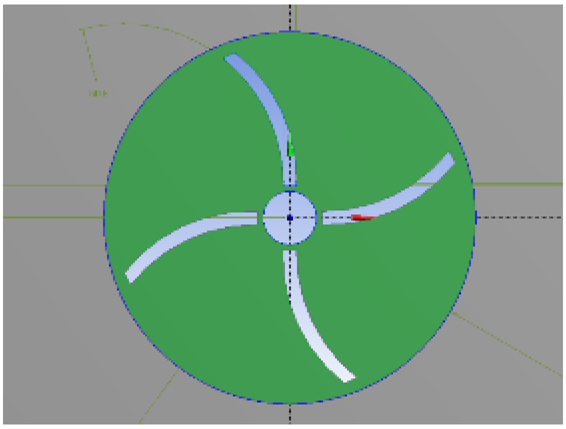

Figure 2: Four-bladed Waterwheel Geometry

2.3 Governing Equations

The transient incompressible flow of water was governed by the conservation equations of mass and momentum. The continuity equation is expressed as

$$\frac{\partial u}{\partial x} + \frac{\partial v}{\partial x} = 0 \tag{1}$$

where

- u = velocity component in the x-direction (m/s)

- v = velocity component in the y-direction (m/s)

The momentum equation is given by

$$\rho\left(\frac{\partial u}{\partial t}\right)+u\left(\frac{\partial u}{\partial x}\right)+v\left(\frac{\partial u}{\partial y}\right)=-\frac{\partial p}{\partial x}+\mu\left(\frac{\partial^2 u}{\partial x^2}+\frac{\partial^2 u}{\partial y^2}\right)+\rho g_x \tag{2}$$

$$\rho\left(\frac{\partial v}{\partial t}\right)+u\left(\frac{\partial v}{\partial x}\right)+v\left(\frac{\partial v}{\partial y}\right)=-\frac{\partial p}{\partial y}+\mu\left(\frac{\partial^2 v}{\partial x^2}+\frac{\partial^2 v}{\partial y^2}\right)+\rho g_y \tag{3}$$

Where

u = velocity in the x-direction (m/s)

v = velocity in the y-direction (m/s)

ρ = density (kg/m^3)

p = pressure (Pa)

μ = dynamic viscosity (Pa·s)

g is the gravitational acceleration vector (m/s^2)

The governing equations were solved using the finite-volume method implemented in ANSYS Fluent.

2.4 Turbulence Modelling

The flow around the rotating blades is characterized by strong streamline curvature, flow separation, wake formation, and transient recirculation regions. To accurately capture these phenomena, the Shear Stress Transport (SST) k–ω turbulence model was employed. The SST k–ω model combines the advantages of the standard k–ω formulation in the near-wall region with the robustness of the (k-ε) model in the outer flow field through a blending function. Consequently, it provides improved prediction of adverse pressure gradients, flow separation, and rotating machinery flows compared with conventional two-equation turbulence models. The transport equations for turbulent kinetic energy (k) and specific dissipation rate (ω) were solved simultaneously throughout the computational domain.

2.5 Computational Mesh

The computational domain was discretized using an unstructured mesh comprising predominantly triangular elements with localized mesh refinement around the runner blades and within the rotating region (Figure 3). Additional refinement was introduced along the blade surfaces and within the expected jet impact zone to accurately resolve steep velocity and pressure gradients. Particular attention was devoted to the interface separating the stationary and rotating domains in order to ensure smooth interpolation of flow variables during the transient sliding mesh calculations (Figure 4). The final computational grid consisted of approximately 75,000 elements and 39,000 nodes, which provided a suitable compromise between numerical accuracy and computational cost considering the available computing resources.

Figure 3: Overall computational mesh

2.6 Mesh Independence Study

A mesh refinement study was conducted qualitatively by comparing torque convergence trends across simulation runs. The selected mesh (75,309 elements) was chosen based on stable torque oscillation after initial transient, acceptable skewness (<0.85 for majority of cells) and consistent periodic torque behaviour across TSR cases. Temporal independence was ensured using a fixed time step of 0.002 s. All cases were simulated up to 4 s of physical time, and results were averaged over the interval 1–4 s to eliminate start-up transients.

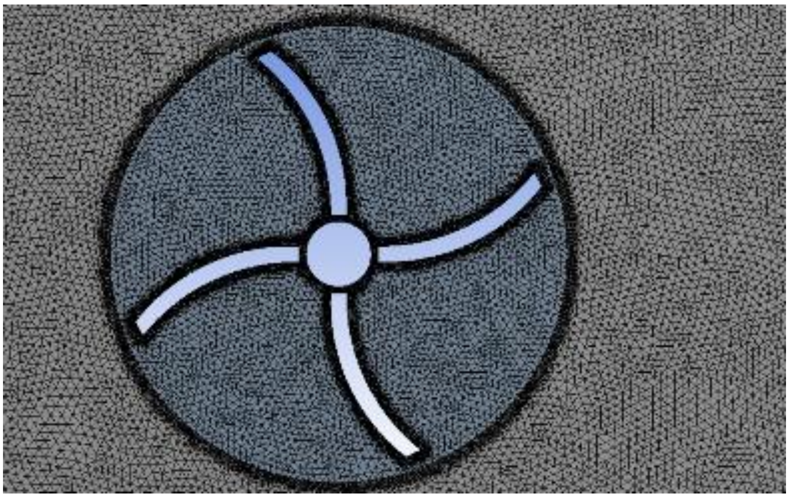

Figure 4: Enlarged Mesh near Blades and Sliding Interfaces

2.7 Boundary Conditions

A uniform velocity inlet boundary condition was prescribed at the inlet opening. The inlet velocity was specified as 3.0 m/s in the positive x-direction using the velocity-component formulation. The incoming flow possessed a turbulence intensity of 5% with a hydraulic diameter of 1.4 m. The outlet boundary was defined as a pressure outlet with zero-gauge pressure, permitting unrestricted discharge of the flow. The upper and lower boundaries of the computational domain were treated as stationary no-slip walls. The rotating runner blades were modelled as no-slip moving walls within the rotating reference frame. The interface between the rotating and stationary regions was implemented using the sliding mesh technique, allowing transient communication of flow variables between the two domains. Gravity was included in the simulations with an acceleration of 9.81 m/s^2 acting in the negative y-direction. Water was considered an incompressible Newtonian fluid having a density of 998.2 kg/m^3.

2.8 Numerical Solution Procedure

Transient simulations were performed using the pressure-based solver available in ANSYS Fluent. Pressure–velocity coupling was achieved using the SIMPLE algorithm. Spatial discretization of momentum and turbulence quantities employed second-order upwind schemes, while transient terms were discretized using a second-order implicit formulation to improve temporal accuracy. Each simulation utilized a time step of 0.002 s with a maximum of twenty iterations per time step. The total simulated flow time was 4.0 s, corresponding to 2000-time steps. Residual convergence of the governing equations was monitored throughout the solution process, while the transient variation of runner torque was simultaneously recorded to ensure stable periodic behaviour before performance evaluation. The numerical procedure is presented in Figure 5.

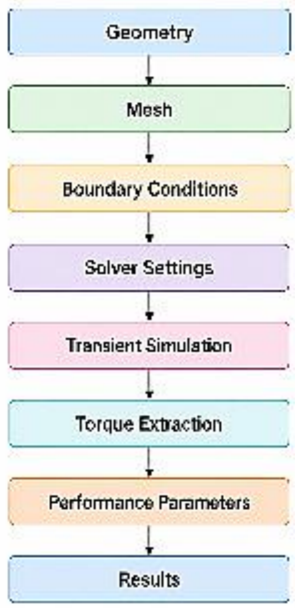

Figure 5: Flow Chart of the Simulation Procedure

2.9 Operating Conditions

Eight operating conditions corresponding to runner rotational speeds of 10, 15, 20, 25, 30, 35, 40, and 45 rpm were investigated. For each operating condition, the inlet velocity was maintained constant at 3.0 m/s, while only the runner rotational speed was varied to obtain different Tip Speed Ratios. This approach enabled direct assessment of the influence of TSR on torque production, shaft power, hydraulic efficiency, and power coefficient.

2.10 Performance Evaluation

The instantaneous torque generated by the runner blades was monitored throughout each transient simulation using the moment report function in ANSYS Fluent. The moment was evaluated about the runner centre with the moment axis aligned with the rotational axis. To eliminate start-up transients, the average torque was computed over the interval between 1.0 s and 4.0 s of simulation time after periodic operation had been established.

The shaft power produced by the runner was determined from

$$P = T\omega \quad (4)$$

where (T) denotes the average runner torque and ω is the angular velocity. The Tip Speed Ratio was calculated as

$$TSR\ (\lambda) = \frac{\omega R}{V} \quad (5)$$

where R is the runner radius and V is the inlet jet velocity. The discharge through the inlet was determined using

$$Q = bhV \quad (6)$$

where b is the runner width, h is the inlet opening height, and V is the inlet velocity. The available hydraulic power was calculated as

$$P_h = \frac{1}{2}\rho Q V^2 \quad (7)$$

Finally, the hydraulic efficiency and power coefficient were evaluated using

$$\eta_h = \frac{T\omega}{\rho g Q H} \quad (8)$$

$$C_P = \frac{T\omega}{\frac{1}{2}\rho A V^3} \quad (9)$$

respectively. These performance indices were subsequently analysed to establish the influence of Tip Speed Ratio on the hydrodynamic behaviour and energy conversion characteristics of the jet-driven four-bladed waterwheel.

3. Results and Discussion

3.1 Influence of Tip Speed Ratio on Torque Characteristics

The average torque obtained at different runner rotational speeds is presented in Table 2, while the variation of average torque with Tip Speed Ratio (TSR) is illustrated in Fig. 6. The results reveal that the hydrodynamic behaviour of the jet-driven four-bladed waterwheel is strongly dependent on the operating TSR.

Table 2: Average Torque Obtained at Different Rotational Speeds and Corresponding Power and Efficiencies

RPM	ω (rad/s)	TSR	Avg. Torque (Nm)	Max Torque (Nm)	Min Torque (Nm)	Mech. Power (W)	Hydraulic Power (W)	η (%)	C_P
10	1.0472	0.244	169.479	307.483	-32.110	177.48	808.54	21.95	0.220
15	1.5708	0.367	131.128	352.620	-114.039	205.98	808.54	25.48	0.255
20	2.0944	0.489	88.904	292.926	-155.090	186.22	808.54	23.03	0.230
25	2.6180	0.611	78.745	322.139	-185.870	206.16	808.54	25.50	0.255
30	3.1416	0.733	135.763	379.421	-121.051	426.51	808.54	52.75	0.528
35	3.6652	0.855	133.613	391.275	-36.779	489.72	808.54	60.57	0.606
40	4.1888	0.977	114.764	369.405	-58.178	480.72	808.54	59.46	0.595
45	4.7124	1.100	90.962	369.687	-78.509	428.58	808.54	53.01	0.530

At the lowest operating speed of 10 rpm (TSR = 0.244), the runner produced the highest average torque of 169.48 Nm. This behaviour is attributed to the relatively low blade peripheral velocity, which allows the incoming water jet to remain in contact with each blade for a longer duration, thereby promoting effective momentum transfer and larger tangential forces. Similar observations have been reported for undershot waterwheels, where lower wheel velocities enhance the interaction time between the incoming flow and the runner, leading to increased torque production (Quaranta & Revelli, 2018).

As the rotational speed increased from 10 to 25 rpm (TSR = 0.244–0.611), the average torque decreased progressively from 169.48 Nm to

78.75 Nm. The reduction indicates that the increasing blade speed reduced the duration of jet–blade interaction, thereby lowering the amount of momentum transferred to the runner during each blade passage. Interestingly, a substantial increase in average torque occurred between 25 and 30 rpm, where the torque increased from 78.75 Nm to 135.76 Nm, followed by 133.61 Nm at 35 rpm.

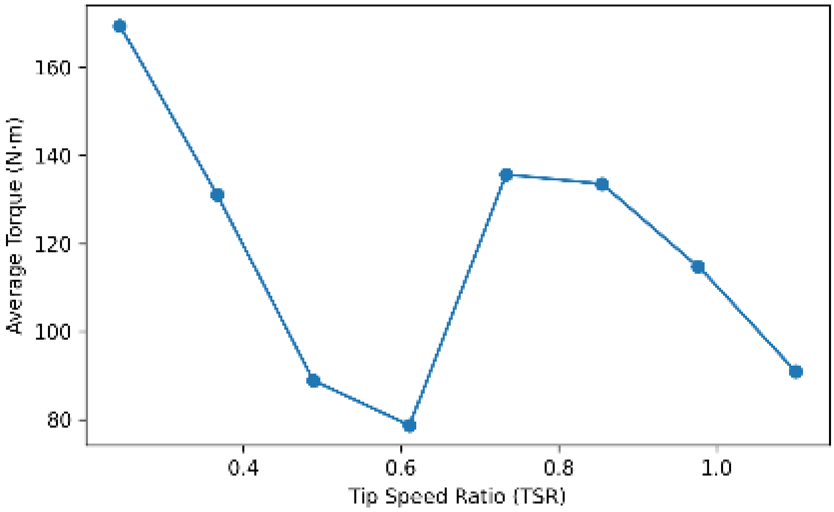

Figure 6: Average torque vs TSR

This behaviour suggests that the runner entered a more favourable hydrodynamic operating regime in which the blade velocity became better matched to the incoming jet velocity. Under these conditions, improved alignment between the blade trajectory and the incoming flow likely enhanced momentum transfer while reducing excessive flow separation.

Beyond 35 rpm, average torque again declined, reaching 114.76 Nm and 90.96 Nm at 40 and 45 rpm, respectively. At higher TSR values, the blades move sufficiently fast that portions of the incoming jet bypass the runner before complete energy transfer can occur, resulting in reduced torque generation. This behaviour is consistent with the classical response of impulse-type hydraulic machines, where an optimum velocity ratio exists for maximum energy extraction.

3.2 Transient Torque Behaviour

The instantaneous torque histories obtained from the transient simulations exhibited periodic oscillatory behaviour throughout the operating cycle (Fig. 7).

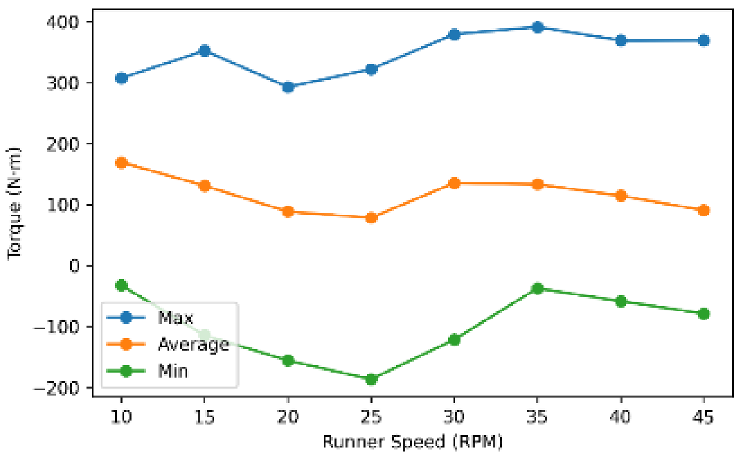

Figure 7: Torque Regime Behaviour

Such oscillations are characteristic of rotating hydraulic machines and arise from the successive interaction of individual blades with the incoming water jet. The periodic nature of the torque signal reflects alternating phases of increasing and decreasing hydrodynamic loading as each blade enters, receives impact from, and subsequently exits the jet region. Positive peaks correspond to maximum momentum transfer immediately after jet impingement, whereas the negative portions of the cycle represent periods during which the runner experiences reduced driving force or temporary hydrodynamic resistance. The maximum instantaneous torque increased from 307.48 Nm at 10 rpm to 391.28 Nm at 35 rpm before decreasing slightly at higher rotational speeds (Figure 8). Meanwhile, the minimum torque values became increasingly negative up to 25 rpm before approaching zero at higher TSRs (Figure 9). This reduction in negative torque at larger TSR values indicates that the higher blade speed reduced the duration of adverse hydrodynamic loading between successive blade impacts.

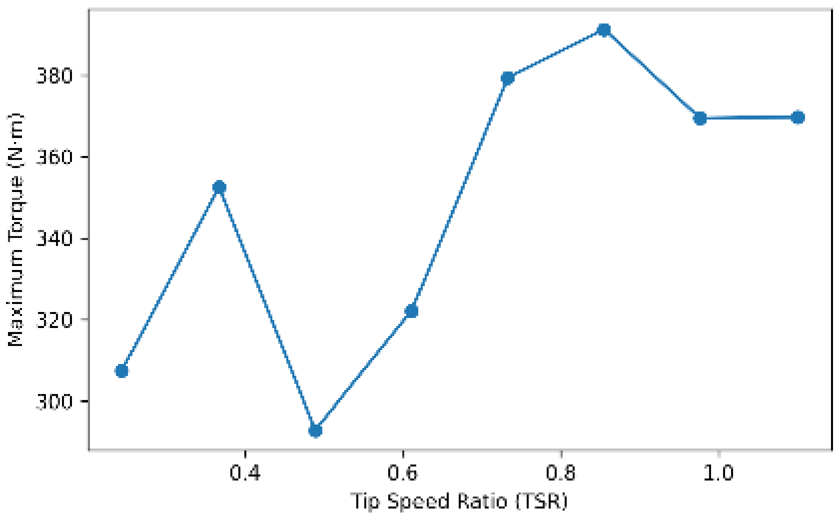

Figure 8: Maximum Torque vs TSR

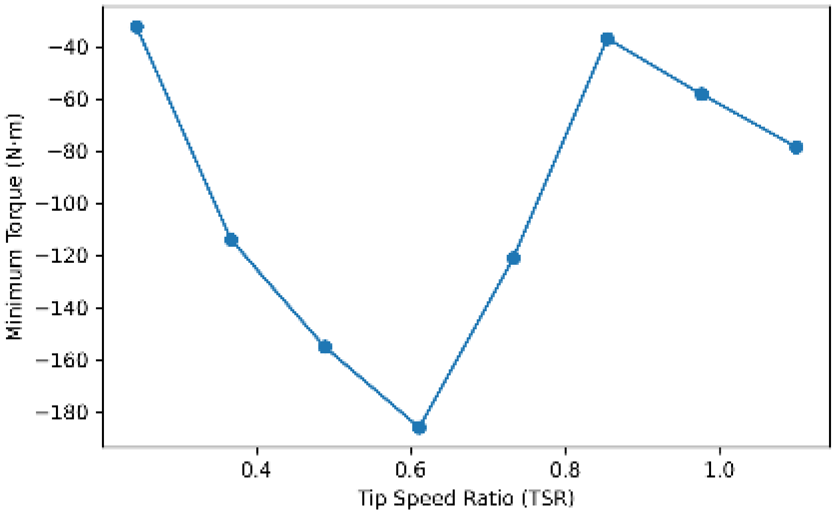

Figure 9: Minimum Torque vs TSR

The observed sinusoidal torque variation confirms the transient nature of jet–blade interaction and demonstrates the necessity of employing sliding mesh transient simulations rather than steady-state approaches for accurate performance prediction.

3.3 Effect of TSR on Mechanical Power

The variation of mechanical power with Tip Speed Ratio is presented in Fig. 10. Unlike average torque, mechanical power did not attain its maximum value at the lowest rotational speed. Mechanical power increased from 177.48 W at 10 rpm to 205.98 W at 15 rpm, followed by a slight reduction to 186.22 W at 20 rpm. A significant increase was subsequently observed as rotational speed increased beyond 25 rpm. The maximum mechanical power of 489.72 W occurred at 35 rpm, corresponding to a TSR of 0.855. Increasing the runner speed beyond this optimum caused power to decrease slightly to 480.72 W at 40 rpm and 428.58 W at 45 rpm.

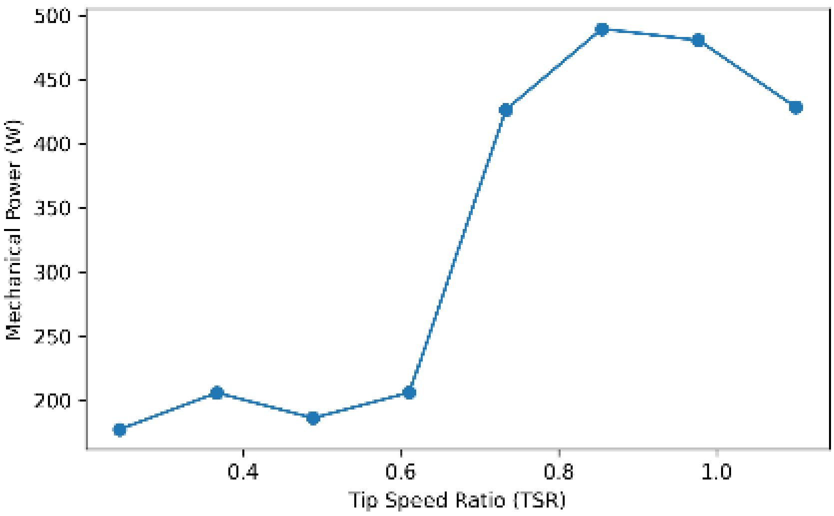

Figure 10: Mechanical Power vs TSR

This trend reflects the combined influence of torque and angular velocity. Although average torque decreases with increasing rotational speed, shaft power is proportional to the product of torque and angular velocity. Consequently, moderate reductions in torque may be compensated by increased rotational speed until the optimum operating condition is reached. The results therefore indicate that maximum power output is achieved at an intermediate TSR rather than at the maximum torque condition.

3.4 Hydraulic Efficiency

The hydraulic efficiency calculated for the investigated operating conditions is presented in Fig. 11. Hydraulic efficiency increased gradually from 21.95% at TSR = 0.244 to 25.50% at TSR = 0.611, indicating progressive improvement in energy conversion efficiency as blade speed approached the optimum velocity ratio. A sharp improvement occurred between TSR values of 0.611 and 0.855, where efficiency increased from 25.50% to 60.57%. This substantial improvement suggests that the incoming jet transferred a significantly larger proportion of its kinetic energy to the runner under these operating conditions. The highest hydraulic efficiency of 60.57% occurred at 35 rpm (TSR = 0.855), after which efficiency declined slightly to 59.46% and 53.01% at TSR values of 0.977 and 1.100, respectively.

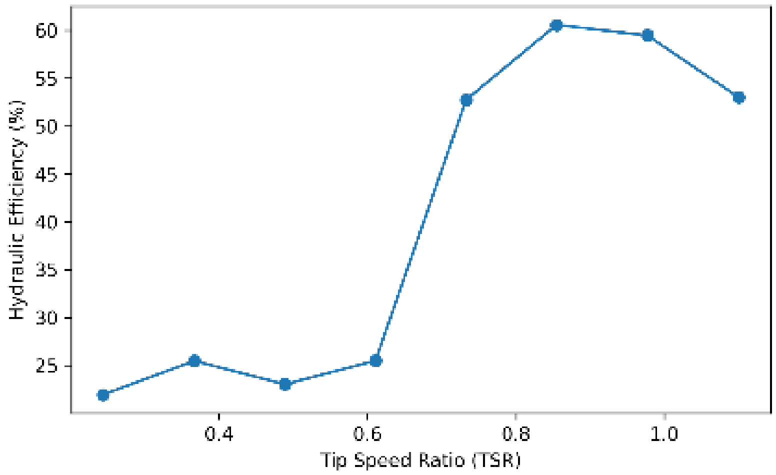

Figure 11: Hydraulic Efficiency vs TSR

The existence of an optimum efficiency point is consistent with previous investigations on waterwheels and impulse turbines, which have shown that maximum energy conversion occurs when the blade peripheral velocity represents an appropriate fraction of the incoming flow velocity (Quaranta & Revelli, 2018).

3.5 Variation of Power Coefficient

The influence of TSR on the power coefficient is shown in Fig. 12. The power coefficient followed a trend similar to that observed for hydraulic efficiency, increasing steadily from 0.220 at TSR = 0.244 to a maximum value of 0.606 at TSR = 0.855. The increase demonstrates improved conversion of the available hydraulic energy into useful mechanical power as the runner approached its optimum operating condition. Following the optimum TSR, the power coefficient decreased to 0.595 and 0.530 at TSR values of 0.977 and 1.100, respectively. The decline indicates that excessive rotational speed reduced the effectiveness of momentum exchange between the incoming jet and the runner blades.

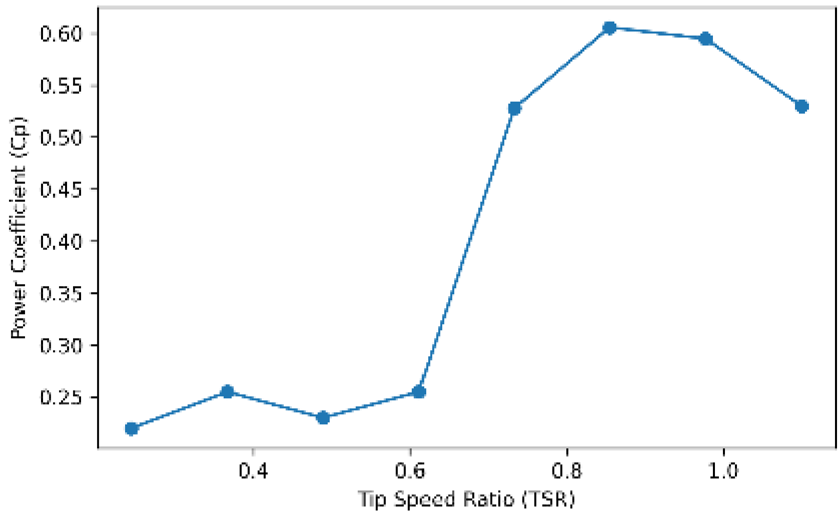

Figure 12: Coefficient of Power vs TSR

The observed optimum TSR agrees with the fundamental operating characteristics of rotating energy conversion systems reported for both hydraulic and aerodynamic turbines, where maximum power extraction occurs within a relatively narrow range of velocity ratios.

3.6 Overall Performance Assessment

The combined results demonstrate that the jet-driven four-bladed waterwheel exhibits distinct operating regimes depending on the Tip Speed Ratio. At low TSR values, the runner generated relatively high torque but comparatively low shaft power due to the limited rotational speed. As TSR increased, the reduction in torque was offset by increasing angular velocity, resulting in improved power production and hydraulic efficiency. The optimum operating condition was obtained at 35 rpm, corresponding to a TSR of 0.855, where the runner produced a mechanical power of 489.72 W, a hydraulic efficiency of 60.57%, and a power coefficient of 0.606.

Beyond the optimum operating condition, further increases in rotational speed caused reductions in average torque, mechanical power, efficiency, and power coefficient. These observations indicate that excessively high blade speeds reduce the effectiveness of jet–blade interaction and consequently diminish energy extraction. Overall, the numerical results demonstrate that Tip Speed Ratio exerts a dominant influence on the hydrodynamic performance of the jet-driven four-bladed waterwheel. The identification of an optimum TSR provides valuable guidance for the design and operational optimization of low-head waterwheel systems intended for decentralized hydropower generation. The results further confirm the suitability of transient CFD simulations for capturing the complex blade–jet interactions governing the performance of jet-driven waterwheels.

4. CONCLUSION

A CFD-based investigation of a jet-driven multi-bladed waterwheel was conducted to evaluate the effect of tip speed ratio on turbine performance. The results show a non-linear relationship between TSR and both torque and power output. Torque decreases initially with increasing TSR, reaches a minimum, and subsequently increases at higher TSR values. Power output increases overall with TSR, reaching a maximum at TSR = 0.733. The study reveals the existence of multiple hydrodynamic operating regimes governed by jet-blade interaction characteristics. These findings provide useful insights for optimizing waterwheel performance in low-head hydropower applications.

5. NOMENCLATURE

Symbol	Definition
TSR (λ)	Tip Speed Ratio
T	Torque (Nm)
P	Mechanical Power (W)
ω	Angular velocity (rad/s)
V	Jet velocity (m/s)
R	Turbine radius (m)
ρ	Fluid density (kg/m^3)
A	Jet cross-sectional area (m^2)
Q	Volumetric flow rate (m^3/s)
Cp	Power coefficient

REFERENCES

(i) Buku, A., & Yandi, N. U. S. P. (2026). An experimental study of the hydrodynamic characteristics of curved blade undershot water wheels for laboratory-scale irrigation. *Engineering, Technology and Applied Science Research*. https://doi.org/10.48084/etasr.17782

(ii) Cleynen, O., Engel, S., Hoerner, S., & Thévenin, D. (2021). Optimal design for the free-stream water wheel: A two-dimensional study. *Energy, 214*, 118880. https://doi.org/10.1016/j.energy.2020.118880

(iii) Asim, M., Muhammad, S., Amjad, M., Abdullah, M., Mujtaba, M. A., Kalam, M. A., Mousa, M., & Soudagar, M. E. M. (2022). Design and parametric optimization of the high-speed pico waterwheel for rural electrification of Pakistan. *Sustainability, 14*(11), 6930. https://doi.org/10.3390/su14116930

(iv) Jiang, H., Yang, J., Wang, X., Qi, B., & Ma, K. (2025). Effects of blade solidity on the transient start-up characteristics of pipeline-type spherical hydraulic turbine. *Proceedings of the Institution of Mechanical Engineers, Part A: Journal of Power and Energy, 239*(3), 480–500. https://doi.org/10.1177/09576509241263472

(v) Quaranta, E., & Revelli, R. (2018). Gravity water wheels as a micro hydropower energy source: A review based on historic data, design methods, efficiencies and modern optimizations. *Renewable and Sustainable Energy Reviews, 97*, 414–427. https://doi.org/10.1016/j.rser.2018.08.033

(vi) Shingala, A., Cleynen, O., Jain, A., Hoerner, S., & Thévenin, D. (2022). Genetic optimisation of a free-stream water wheel using 2D computational fluid dynamics simulations points towards design with fully immersed blades. *Energies, 15*(10), 3723. https://doi.org/10.3390/en15103723

(vii) Štigler, J. (2022). Overshot water wheel efficiency measurements for low heads and low flowrates. *EPJ Web of Conferences, 269*, Article 01058. https://doi.org/10.1051/epjconf/202226901058

(viii) Paudel, S., Weber, M., Geyer, D., & Saenger, N. (2022). Experimental and numerical study of Zuppinger water wheel model. In *Proceedings of the Institution of Civil Engineers-Water Management* (Vol. 175, No. 4, pp. 206-216). Thomas Telford Ltd.

(ix) Basar, M. F., Zulkarnain, I. A., & Sopian, K. (2025). A Comprehensive Analysis of Waterwheel Technologies for Pico Hydropower: Evolution, Performance, and Optimization Strategies. *International Research Journal of Multidisciplinary Scope*, *6*(03), 580-599.